

# Exploiting nanogroove-induced cell culture anisotropy to advance *in vitro* brain models

Cite as: J. Vac. Sci. Technol. B **37**, 061802 (2019); <https://doi.org/10.1116/1.5119687>

Submitted: 11 July 2019 . Accepted: 10 September 2019 . Published Online: 01 October 2019

 Alex Bastiaens, Jean-Philippe Frimat, Teun van Nunen, and Regina Luttge

## COLLECTIONS

Paper published as part of the special topic on [Conference Collection: The 63rd International Conference on Electron, Ion, and Photon Beam Technology and Nanofabrication \(EIPBN 2019\)](#)

 This paper was selected as an Editor's Pick



[View Online](#)



[Export Citation](#)



[CrossMark](#)

## ARTICLES YOU MAY BE INTERESTED IN

[Brilliant mid-infrared ellipsometry and polarimetry of thin films: Toward laboratory applications with laser based techniques](#)

Journal of Vacuum Science & Technology B **37**, 060801 (2019); <https://doi.org/10.1116/1.5122869>

[Reflective metamaterial polarizer enabled by solid-immersion Lloyd's mirror interference lithography](#)

Journal of Vacuum Science & Technology B **37**, 061801 (2019); <https://doi.org/10.1116/1.5119138>

[Multiple replication of hierarchical structures from polymer masters with anisotropy](#)

Journal of Vacuum Science & Technology B **37**, 061601 (2019); <https://doi.org/10.1116/1.5120881>



The banner features the AVS logo (a stylized globe with horizontal lines) and the text "Advance your science and career as a member of AVS". A yellow button on the right says "LEARN MORE >".



# Exploiting nanogroove-induced cell culture anisotropy to advance *in vitro* brain models

Alex Bastiaens, Jean-Philippe Frimat, Teun van Nunen, and Regina Luttge<sup>a)</sup>

Neuro-Nanoscale Engineering Group, Microsystems Section, Department of Mechanical Engineering and Institute of Complex Molecular Systems (ICMS), Eindhoven University of Technology, Eindhoven 5612AZ, The Netherlands

(Received 11 July 2019; accepted 10 September 2019; published 1 October 2019)

A new generation of *in vitro* human brain models is vital to surpass the limitations of current cell culture platforms and animal cell lines in studying brain function and diseases. Brain-on-chip technology can generate well-defined and reproducible platforms to control the cellular microenvironment for *in vivo*-like, organized brain cell cultures. Previously, the authors investigated differentiation and network organization of the neuroblastoma SH-SY5Y cell line on nanogrooved substrates, showing that nanogroove guidance of neuronal outgrowths is dependent on nanogroove dimensions. Further, increased orientation of neurites was positively correlated to the differentiation of SH-SY5Y cells. However, as mimicking brain structure alone is insufficient, here, the function of the neuronal cell network as dependent on surface topography and material stiffness is investigated. A generalized replication protocol was developed to create similar nanogrooved patterns in cell culture substrates from different materials, specifically polydimethylsiloxane (PDMS) and Ostemere. Experiments using calcium imaging, where calcium fluxes across membranes are visualized as an indication of action potentials in neuronal cells, were performed with differentiated SH-SY5Y cells and human induced pluripotent stem cell-derived neuronal cells (hiPSCNs) on flat versus nanogrooved substrates to study the network function. Calcium live-imaging was performed and results for experiments with SH-SY5Y cells and hiPSCNs showed that nanogrooved PDMS substrates trended toward increased cellular activity and neuronal cell network connectivity. For future investigation of compatible substrate materials in combination with the effect of material stiffness on the cells, nanogrooved Ostemere substrates were demonstrated to faithfully replicate for use in neuronal cell cultures using nanogrooved substrates. First experiments into the neuronal cell function using stem cells described here aid toward elucidating the effect of nanotopographical and mechanical properties and their benefits toward advancing *in vitro* neuronal cell models both in form and function. Overall, the results indicate, in conjunction with the previous findings on neuronal outgrowth guidance, that anisotropy as introduced by nanogrooved substrates can have a controllable and potentially beneficial influence on neuronal cell cultures. © 2019 Author(s). All article content, except where otherwise noted, is licensed under a Creative Commons Attribution (CC BY) license (<http://creativecommons.org/licenses/by/4.0/>). <https://doi.org/10.1116/1.5119687>

## I. INTRODUCTION

A new generation of advanced *in vitro* human brain models is vital to surpass the limitations of current cell culture platforms and animal cell lines in studying brain function and brain diseases.<sup>1,2</sup> These new models can be achieved using brain-on-chip technology, employing micro- and nanofabrication to create well-defined, controllable, and reproducible platforms with a cellular microenvironment that allows for *in vivo*-like, spatially organized brain cell culture.

In general, cells interact with the cellular microenvironment. Studies have shown that, as part of the physical micro-environment, nanotopography and anisotropical patterns at the nanoscale can influence cell morphology, adhesion, and provide guidance to cellular structures.<sup>3,4</sup> More specifically,

current research has shown the importance of nanotopography and environmental anisotropy to examine the response of brain cells.<sup>5</sup> Nanoscale anisotropy introduced by nanotopography can guide neuronal cell network architecture and enhance differentiation of neuronal cells, thereby enhancing *in vitro* cell models<sup>6–9</sup> and intracortical interfacing.<sup>10</sup>

Previously, our group studied the interaction between brain cells and nanoscale features, in which a range of nanogrooved patterns with different dimensions was fabricated in different materials, to explore the benefits of these patterns. It has been shown that different patterns elicit different responses from both astrocytes in primary rat cortical cells<sup>11</sup> and the neuroblastoma cell line SH-SY5Y (Ref. 12) in the amount of guidance perceived by the cells. Additionally, the mechanical properties of the nanogrooved substrate material, here silicon, nanoresist, or polydimethylsiloxane (PDMS) with differing mixing ratios of elastomer and curing agent, altered the extension of neuronal outgrowths.<sup>13</sup> Automated image based screening analysis was developed to study large image data sets to process morphological output parameters.

Note: This paper is part of the Conference Collection: The 63rd International Conference on Electron, Ion, and Photon Beam Technology and Nanofabrication (EIPBN 2019).

<sup>a)</sup>Electronic mail: r.luttge@tue.nl



The analysis revealed that nanogrooves with ridges that are relatively small compared to the pattern periodicity showed a more consistent and a higher guidance effect on neuronal outgrowths. Further, SH-SY5Y cells showed positive correlations between the neuronal outgrowth guidance effect of nanogrooves, differentiation toward neuronal cells and the outgrowth length.<sup>14</sup>

Our previous data, collected from fixed and immunostained cultures, have shown the influence of nanogrooved patterns on morphological parameters. However, the influence on the electrophysiological behavior of cells and the neuronal cell network were yet to be studied. Here, we present results of a first functional analysis for SH-SY5Y and human induced pluripotent stem cell-derived neuronal cells (hiPSCNs) cultured on nanogrooved substrates, as compared to cultures on flat substrates. Electrophysiological activity of cells was recorded by calcium imaging and analyzed using the in-house developed calcium imaging analysis software CALIMA.<sup>15</sup>

In an effort to be able to study other materials, in particular, to introduce ranges of mechanical properties beyond the capacity of PDMS, we also investigated approaches to replicate nanogrooved patterns into Ostemere. Ostemere is a biocompatible material of increasing interest in microfluidics and organ-on-chip<sup>16</sup> with different material and mechanical properties from PDMS, such as a stiffness of 2.3 GPa when fully cured,<sup>17</sup> for which pattern transfer at the nanoscale should have high fidelity. This material would complement the findings observed in PDMS and add to our database of nanogrooved substrates for use in brain-on-chip technology.

Here, the main aim was to investigate how the anisotropy introduced by nanogrooves influences activity in neuronal cell and neuronal cell networks as seen from intracellular calcium fluxes. From a fabrication perspective, we have

shown a fabrication process by which nanogrooved patterns could be replicated into Ostemere and potentially various materials other than PDMS, by means of which it becomes possible to decouple the effects of mechanical properties and nanotopography on neuronal cell activity derived from the calcium flux profile. Based on this knowledge, input parameter design can be optimized toward the bottom-up engineering of neuronal cell network form and function. These anisotropic features at the nanoscale can then be incorporated, thereby advancing the structure and robustness of brain-on-chip platforms and present us with the formation of *in vivo*-like brain cell cultures.

## II. EXPERIMENT

### A. Nanogrooved substrate fabrication

#### 1. Fabrication of a durable nanogrooved cyclic olefin copolymer mold

The fabrication details for the nanoresist scaffolds were published by Xie and Luttge.<sup>11</sup> In brief, the nanoresist was patterned using jet and flash imprint lithography on a standard double-sided polished 100 mm diameter silicon wafer [Fig. 1(a)]. The wafer was first coated with a bottom antireflective coating (DUV30J, Brewer Science) layer using a quartz master kindly provided by the Bijkerk group at the University of Twente. The nanogrooved patterns had dimensions in the range of 200–2000 nm pattern periodicity, a ridge width of 100–1340 nm, and a height of 118 nm. Subsequently, the nanoresist patterns were used directly as a template in thermal nanoimprint lithography, creating a negative copy in cyclic olefin copolymer (COC; optical grade TOPAS 8007S-04, Kunststoff-Zentrum) using a thermal nanoimprint lithography system (EITRE 6, Obducat) at 108 °C and

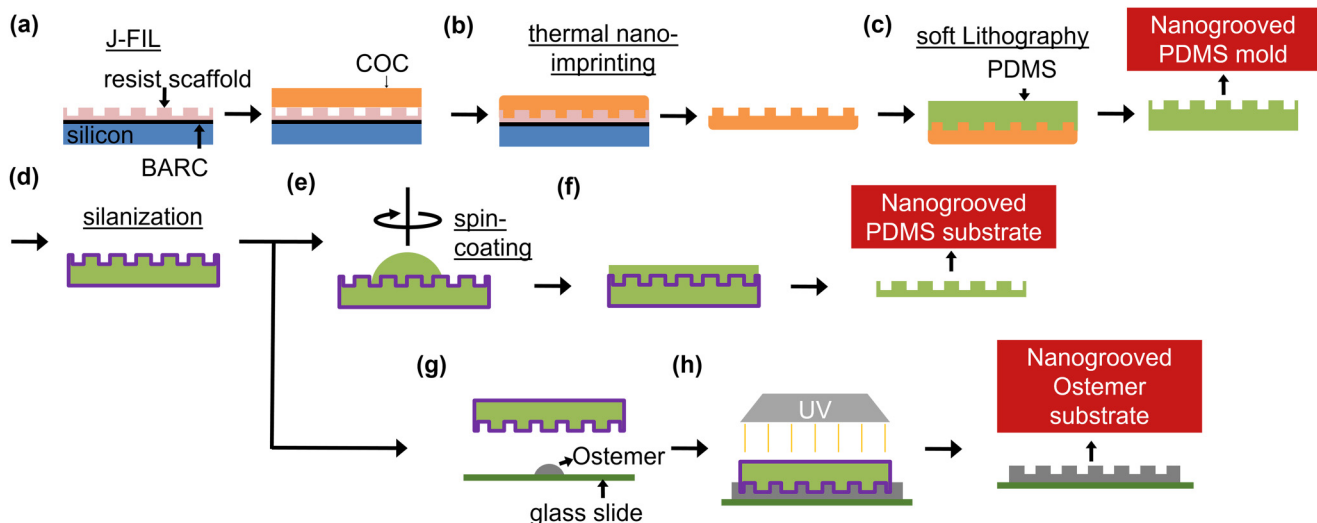


FIG. 1. Fabrication of nanogrooved substrates for neuronal cell culture experiments. A nanogrooved mold was fabricated by means of a fabrication process consisting of (a) Jet and Flash Imprint Lithography in resist, which was deposited on a bottom antireflective coated silicon wafer, followed by (b) thermal nanoimprinting in COC and (c) soft lithography in PDMS. (d) The PDMS mold was subsequently silanized for replication into different materials. Specifically, (e) PDMS was spincoated onto the silanized mold to create a 100 μm layer, (f) which was cured in an oven at 65 °C for 4 h, resulting in a nanogrooved PDMS cell culture substrate. Alternatively, (g) Ostemere components A and B were mixed at a 1.09:1 ratio and poured onto a glass slide, with the silanized mold pressed into the Ostemere. Subsequently, (h) Ostemere was cured in a two-step process of UV exposure followed by thermal curing at 110 °C, resulting in a nanogrooved Ostemere cell culture substrate.

applying a pressure of 4 MPa [Fig. 1(b)]. After cooling the COC to room temperature, it was peeled off the nanoresist. The COC acted as a primary nanogrooved mold for further replication of nanogrooved cell culture substrates.

## 2. Replica molding of nanogrooves into polydimethylsiloxane cell culture substrates

To ensure the longevity of the COC mold, replication was performed in secondary molds of PDMS prior to replication of the nanogrooves into the final nanogrooved cell culture substrates [Fig. 1(c)]. Considering that a large number of cell culture substrates would be utilized, the risks of materials clogging the nanogrooves due to the repeated use of the original COC mold are greatly reduced. PDMS elastomer and curing agent were mixed at a 10:1 ratio and degassed for 10 min using a vacuum desiccator. PDMS was spincoated at 500 rpm for 60 s to achieve a 100  $\mu\text{m}$  layer of PDMS, which was cured in an oven at 65 °C for 4 h and peeled off for the nanogrooved PDMS cell culture substrate in these experiments. Further, a layer of approximately 5 mm was poured on the COC mold. After which, PDMS on the COC mold was placed in a vacuum desiccator for 10 min to ensure no gas would be trapped near the PDMS–COC interface. Subsequently, the PDMS was placed in an oven at 65 °C for 4 h to ensure the PDMS was fully cured.

The secondary mold in PDMS was peeled off the COC, and chemical vapor deposition was used to silanize the nanogrooved surface for further replication into Ostemere cell culture substrates [Fig. 1(d)]. First, the PDMS mold was treated with an oxygen plasma using the EMITECH K1050X plasma ashing at 20 W for 30 s. Subsequently, a 10  $\mu\text{l}$  drop of 1H, 1H, 2H, 2H-perfluorodecyl-triethoxysilane (658758, Sigma Aldrich, Zwijndrecht, The Netherlands) was placed on a small aluminum tray next to the nanogrooved PDMS mold inside a vacuum desiccator. The materials were then left overnight in a vacuum inside a fume hood.

## 3. Replica molding of nanogrooves into Ostemere cell culture substrates

Nanogrooved cell culture substrates in Ostemere (OSTEMER 322 Crystal Clear, Mercene Labs, Stockholm, Sweden) were made by soft lithography on the secondary PDMS mold. Ostemere components A and B were mixed at a 1.09:1 weight ratio and kept in a UV-free environment due to its photocuring nature. Approximately 100  $\mu\text{l}$  of Ostemere was poured on a thin microscopy slide; after which, the PDMS mold was placed on top [Fig. 1(g)]. After degassing for 10 min in a vacuum desiccator, the materials were UV-cured at 8.1 W for 60 s to perform the primary curing step for Ostemere [Fig. 1(h)]. Subsequently, the materials were placed on a hot plate for 1 h at 110 °C to perform the secondary curing step for Ostemere. The PDMS mold was peeled off, leaving a nanogrooved Ostemere cell culture substrate.

To replicate nanogrooved PDMS from the same secondary PDMS mold as Ostemere, a layer of PDMS was spin-coated at 500 rpm for 60 s to achieve a 100  $\mu\text{m}$  layer of

PDMS [Fig. 1(e)], which was cured in an oven at 65 °C for 4 h and peeled off for the nanogrooved PDMS cell culture substrate [Fig. 1(f)]. As nanogrooved PDMS substrates were already replicated as described in Subsection II A 2, the nanogrooved PDMS substrates derived from the secondary PDMS mold were not used for cell culture.

## B. Atomic force microscopy of nanogrooved substrates

Atomic force microscopy (AFM) was used to characterize the topography of the nanogrooved patterns in PDMS and Ostemere to assess the pattern replication fidelity of these substrates. The XE-100 (Park Systems) was used in tapping mode using a noncontact cantilever (PPP-NCHR, Park Systems) in conjunction with XEP software (Park Systems) to record the AFM data. Analysis of the data was conducted using GWYDDION software.<sup>18</sup>

## C. Neuronal cell culture

### 1. SH-SY5Y cell culture

Nanogrooved patterns with 1000 nm pattern periodicity and 230 nm ridge width were selected for cell culture experiments. Subsequently, they were cut from the PDMS substrates and placed into wells, alongside wells containing flat PDMS and wells without substrates as controls, for neuronal cell network function on flat substrates. PDMS substrates were sterilized with 70% ethanol for 5 min. After which, the ethanol was evaporated by placing the substrates in an oven at 65 °C for 1 h. The PDMS mold was treated with an oxygen plasma using the EMITECH K1050X plasma ashing at 20 W for 30 s. To coat the PDMS, 10  $\mu\text{g cm}^{-2}$  fibronectin (FC010, Sigma Aldrich) in phosphate buffered saline (PBS; LO BE02-017F, Westburg) was applied for 30 min. Following, the fibronectin coating was aspirated from the PDMS substrate, and the cell suspension was immediately dispensed on the surface.

The human neuroblastoma SH-SY5Y cell line (94030304, Sigma Aldrich) was cultured on the PDMS substrates as a reductionist model of brain cells. Cells were stored in cryovials in liquid nitrogen, thawed, and plated in a T75 flask until the cell culture reached 70%–80% confluence. Growth medium was used, composed of Dulbecco's modified Eagle's medium and Ham's F12 medium at a 1:1 ratio (L0093-500, VWR) supplemented with 10% fetal bovine serum (SFBS lot 11113, Bovogen) and 1% penicillin/streptomycin (LODE17-602E, Westburg). The cells were kept in an incubator at 37 °C and 5% CO<sub>2</sub>. At 0 days *in vitro* (DIV), cells were seeded onto the fibronectin-coated substrates in growth medium at 20 000 cells  $\text{cm}^{-2}$ . After at least 3 h, during which cells could adhere to the PDMS cell culture substrate, the medium was replaced with growth medium supplemented with 10  $\mu\text{M}$  retinoic acid (R2625, Sigma Aldrich) to initiate neuronal differentiation, maintained for 72 h,<sup>19,20</sup> and refreshed after 36 h. Subsequently, cell differentiation was further enhanced by adding growth medium with 50 ng  $\text{ml}^{-1}$  brain-derived neurotrophic factor (B2795,

Sigma Aldrich) for 72 h,<sup>21,22</sup> with medium being refreshed after 36 h. After differentiation, cells were kept in growth medium until used for calcium imaging, refreshing the medium every 48 h.

To assess the contact guidance of the SH-SY5Y cells due to the underlying nanogrooved patterns, brightfield microscopy images were taken of the cell culture prior to calcium imaging. Subsequently, the images were assessed for the preferred orientation of cellular features, if any, using the Directionality plugin of the image analysis software FIJI,<sup>23</sup> returning histograms on the distribution of feature orientations within an image.

## 2. hiPSCN cultures

Nanogrooved patterns with 1000 nm pattern periodicity and 230 nm ridge width were selected for hiPSCN culture experiments. Subsequently, they were cut from the PDMS substrates and placed onto ibidi slides (81506, ibidi GmbH, Gräfelfing, Germany), alongside wells containing flat PDMS and wells without substrates, prior to hiPSCN cultures. The wells without nanogrooved substrates served as controls for neuronal cell network function on flat substrates. The nanogrooved PDMS was treated with an oxygen plasma using the EMITECH K1050X plasma asher at 20 W for 30 s. Subsequently, substrates were sterilized for 5 min using 70% ethanol and washed four times using deionized water prior to adding the cell culture coating. Nanogrooved Ostemer substrates on glass slides also contained patterns with a pattern periodicity of 1000 nm and a ridge width of 230 nm. The Ostemer substrates were placed in well plates and sterilized for 5 min using 70% ethanol. After which, the substrates were washed four times using deionized water prior to adding the cell culture coating.

To generate a population of cortical neuronal cells, hiPSCNs (ax0015, Axol Bioscience, Cambridge, UK) were used according to the manufacturer's guidelines. No prior cell culture expansion was performed, and the cells were used immediately for experiments with the prepared cell culture substrates. The PDMS and Ostemer substrates were precoated with SureBond-XF coating (Axol Bioscience) diluted in Dulbecco's phosphate buffered saline (DPBS; L0615-500, VWR) and incubated at 37 °C and 5% CO<sub>2</sub> for 1 h prior to cell seeding. Cells were thawed, added in a drop-wise manner to an Eppendorf tube containing 10 ml of prewarmed, 37 °C, Neural Expansion-XF Medium (Axol Bioscience), and centrifuged at 200×g for 5 min. Subsequently, the medium was removed, and the cells were resuspended in Neural Plating-XF Medium (Axol Bioscience). Cells were counted using the NucleoCounter NC-200 to determine cell density. Cells were plated at a density of  $1.5 \times 10^5$  cells cm<sup>-2</sup> and incubated at 37 °C and 5% CO<sub>2</sub>. After 24 h, 50% of the medium was replaced with Neural Maintenance-XF Medium (Axol Bioscience). The change in medium allowed the cells to recover from thawing and seeding. The full medium volume was exchanged with Neural Differentiation-XF Medium (Axol Bioscience) following another 24 h. To create a population of cortical

neurons, 50% of the medium volume was refreshed with Neural Differentiation-XF Medium every 48 h until 10 DIV. After 10 DIV, 50% of the medium was refreshed using Neural Maintenance-XF Medium every 48 h. Cells were kept in culture until used for calcium imaging. For immunofluorescence staining, cells were washed twice using PBS for 5 min. After which, the cells were fixed using 3.7% formaldehyde for 30 min. Subsequently, fixed cells were washed twice with PBS for 5 min and stored in a fridge until used in the immunofluorescence staining assay.

## D. Calcium imaging and analysis

Calcium imaging was performed on the neuronal cell cultures as an indication of electrophysiological activity. Action potentials produced by neuronal cells are dependent on a flux of calcium ions across the cell membrane. Hence, by binding fluorescent probes to the intracellular calcium ions, the flux can be visualized and activity recorded. The Fluo-4 calcium imaging kit (F10489, ThermoFisher Scientific, Eindhoven, The Netherlands) was used to add the fluorescent probes to the cell cultures.

For SH-SY5Y, calcium imaging was performed at 14 and 21 DIV. A calcium loading buffer was prepared by adding 10 µl Powerload concentrate and 1 µl of Fluo-4 AM to an Eppendorf tube and vortexing for 1 min. Subsequently, 1 ml of the SH-SY5Y growth medium was added, and the solution was mixed by gentle shaking. Cells were washed once with PBS prior to adding the calcium loading buffer. Cells were incubated at 37 °C and 5% CO<sub>2</sub> for 30 min, followed by incubation for 30 min at room temperature covered in aluminum foil. The cell culture was washed once with growth medium. After which, 1 ml of growth medium supplemented with 50 µl of Neuro Backdrop Background Suppressor solution was added to the cell culture for calcium imaging. Recordings were made using the EVOS FL fluorescent microscope at 20× magnification with a fluorescence filter capable of visualizing Fluo-4 fluorescent probes. A 10 min time-lapse was recorded, with image acquisition every 10 s.

For hiPSCNs, calcium imaging was performed at 9 and 13 DIV. The calcium loading buffer was added similarly to the SH-SY5Y cells; however, the maintenance medium for hiPSCNs was used instead of the SH-SY5Y growth medium. Recordings were also performed using the same settings as the SH-SY5Y cells.

To analyze the calcium imaging recordings for both cell types on the nanogrooved PDMS and flat substrates, an in-house developed calcium imaging analysis software called CALIMA was used.<sup>15</sup> The CALIMA software allows the user to detect cell bodies and cell intensity over time, analyze spiking events within the intensity profiles, correlate spiking events between cells based on timing and distance, and to create a spatiotemporal visualization of network connectivity based on these correlated spiking events. Further, all of the generated data for each step can be exported to .csv files, allowing for further analysis in other software.

## E. Immunofluorescence staining and microscopy

To determine whether an increase in activity of hiPSCNs was linked to an increase in synapses, synaptophysin staining was performed on 13 DIV-fixed hiPSCNs. Briefly, 0.5% Triton X-100 (1.086.031.000, Merck Millipore, Schiphol-Rijk, The Netherlands), diluted in DPBS, was added to the fixed hiPSCNs for 15 min to permeabilize the cells. Subsequently, a blocking solution of 10% horse serum (HS, 16050-122, Thermo Fisher Scientific) was applied for 15 min, followed by overnight incubation of the primary antibody anti-synaptophysin (SAB4502906, Sigma Aldrich) at a 1:200 dilution in a DPBS solution with 10% HS. The secondary donkey anti-rabbit Alexa 647 antibody (711-605-152, Jackson ImmunoResearch, Cambridge, UK) was incubated for 2 h at a 1:200 dilution in DPBS with 1% HS, two drops of Nucblue (R37605, ThermoFisher Scientific) per milliliter, and two drops of Actingreen (R37110, ThermoFisher Scientific) per milliliter. Cells were washed three times with DPBS in between each step. Images were produced using the EVOS FL microscope.

## III. RESULTS AND DISCUSSION

### A. Nanogrooved substrate fidelity

Nanogrooves were measured for both PDMS and Ostemere substrates, for at least area sizes of  $5 \times 5 \mu\text{m}^2$  and  $256 \times 256$  pixels as shown in Fig. 2. Patterns for the PDMS substrates had a pattern depth of  $106 \pm 1.31$  nm, a pattern periodicity of  $985 \pm 0.76$  nm, and a ridge width of  $253 \pm 14.9$  nm ( $n = 4$ ). Patterns for the Ostemere substrates had a pattern depth of  $92 \pm 2.10$  nm, a pattern periodicity of  $986 \pm 1.04$  nm, and a ridge width of  $270 \pm 12.3$  nm ( $n = 4$ ).

These results show that nanogrooved patterns at these dimensions can be faithfully replicated for different materials, such as PDMS and Ostemere. Ideally for both substrates, the secondary PDMS mold would be used for replication as shown in Fig. 1. While the overall dimensions of the nanogrooves were retained, the ridges did show limited replication at the edges. The ridges became curved, which may indicate that some material may have gotten stuck during peeling or that the nanogrooves did not fill fully when the substrate materials in their liquid form were poured onto the mold. Extending the duration of degassing, or alternative treatments of the PDMS mold such as atomic layer deposition of other inert or repulsive molecules other than silane, may improve upon these limitations.

### B. Nanogroove influence on neuronal cell networks

#### 1. Neuronal cell culture on nanogrooved substrates

During cell culture, both SH-SY5Y cells and hiPSCNs were analyzed for cell survival and morphological changes that indicate neuronal differentiation prior to performing calcium imaging experiments (Fig. 3). SH-SY5Y cells showed a change in morphology from round on flat substrates to oval-shape and parallel directionality on nanogrooves, indicating the guidance effect of the nanogrooves on the cells [Figs. 3(a) and 3(b)]. This qualitative indication

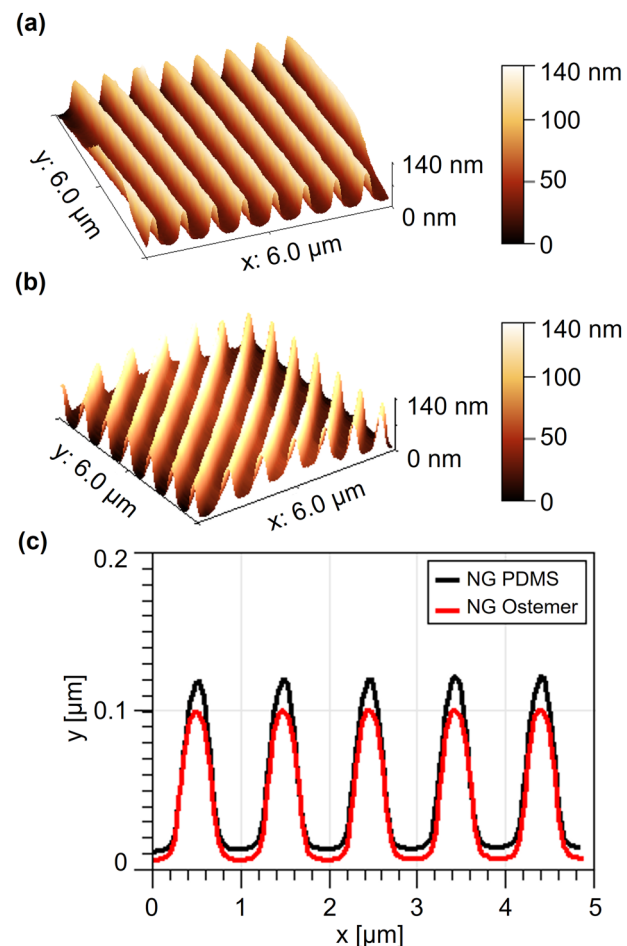


FIG. 2. Nanogrooved (a) PDMS and (b) Ostemere cell culture substrates were measured using atomic force microscopy to determine the fidelity of pattern transfer during the replication process as described in Sec. II A. Nanogroove patterns had a pattern periodicity of 1000 nm and a ridge width of 230 nm. (c) The line profile for the nanogrooved PDMS and Ostemere substrates, showing similar retained profiles of pattern periodicity, pattern height, and ridge width.

is confirmed by calculating the directionality of the features seen in these images. The histogram for feature orientations seen for cells on flat PDMS [Fig. 3(c)] shows no preferred direction, whereas the cells on nanogrooved PDMS [Fig. 3(d)] show a preferred direction of approximately  $120^\circ$ . The angle at which cellular features preferably orient on the nanogrooved PDMS coincides with the angle at which the nanogrooves are in the image. Further, neuronal outgrowths were visible, showing successful neuronal differentiation of the SH-SY5Y cells.

For hiPSCNs, cell culture was unsuccessful when performed on the Ostemere substrates (see Fig. S1 in the supplementary material<sup>30</sup>). The SureBond coating supplied by the manufacturer is optimized for coating glass substrates for hiPSCNs adhesion, which appears not to be chemically compatible with unmodified Ostemere, thereby reducing the coating efficiency. Alternatively, reacting the Ostemere with silicon oxide groups after curing and prior to coating to mimic glass, or using atomic layer deposition of a silicon oxide layer on top of the Ostemere, could provide the correct chemical interface for adherence.

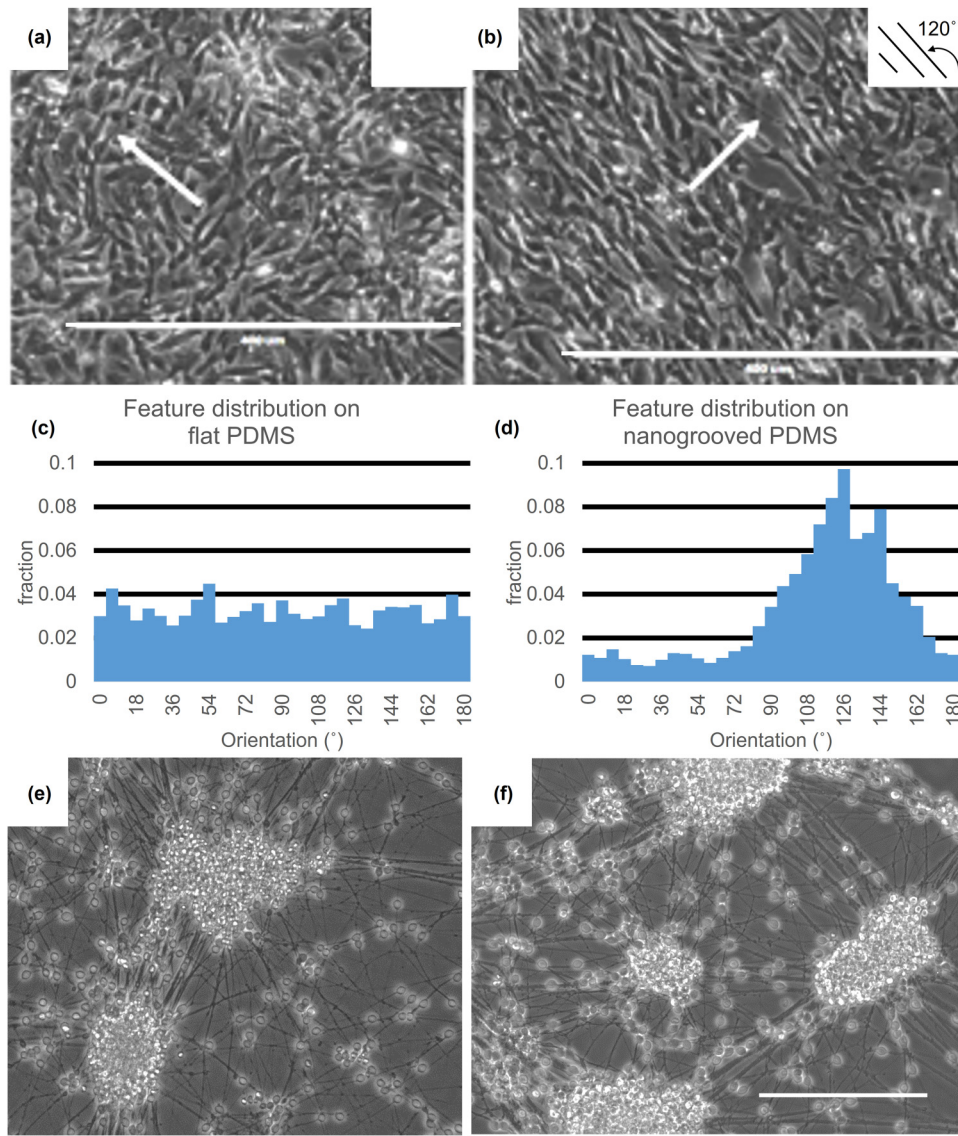


FIG. 3. Examples of SH-SY5Y and hiPSCN cultures on PDMS substrates. SH-SY5Y cells on (a) flat PDMS and (b) nanogrooved PDMS after 7 DIV showed differentiation and neuronal outgrowths (white arrows). The direction of the nanogrooved pattern is indicated on the top right corner of (b), with lines parallel to direction to the nanogrooves of the PDMS substrate at approximately a 120° angle from the horizontal axis. The directionality of the cellular features seen in (a) and (b) was calculated using the Directionality plugin in Fiji for both flat PDMS (c) and nanogrooved PDMS (d), resulting in histograms for the distribution of feature orientations. Culture of hiPSCNs on (e) flat PDMS and (f) nanogrooved PDMS after 13 DIV. All scale bars denote 400 μm. Image brightness was increased for all images by 20%–40% for visualization purposes.

Culture of hiPSCNs on the PDMS substrates and in the control wells of ibidi slides was successful, with cell survival and differentiation visible from several hours after seeding. Over the course of several days, the cells did migrate, and most cells formed clusters [Figs. 3(e) and 3(f)], as opposed to the retained in the SH-SY5Y cell culture. Neuronal outgrowths extended several hundred micrometers over the course of several days, also forming larger bundles of outgrowths between clusters of cells, as opposed to the relatively shorter and fewer neurites for SH-SY5Y cells.

## 2. Neuronal cell activity

To quantify the effect of nanogrooved substrates on the activity of SH-SY5Y cells and hiPSCNs, calcium imaging

recordings were analyzed using CALIMA software as shown in Fig. 4. First, detection filters were applied to determine an overlay for each individual cell [Figs. 4(a)–4(c)]. For each cell, the intensity over the duration of the recording was measured. Following, thresholds were applied to distinguish spiking events, which indicate electrophysiological behavior of cells, from background noise. This was visually indicated using a spatiotemporal map of the spiking events [Figs. 4(d)–4(f)]. Subsequently, the correlation was calculated for each cell regarding synchronous spiking to create a map of the cell network connectivity [Figs. 4(g)–4(i)]. The cell network connectivity results are shown in Subsection III B 3.

From the images in Fig. 4, a qualitative observation can be made with regard to the differences between SH-SY5Y cells on flat glass [Figs. 4(a), 4(d), and 4(g)], flat PDMS

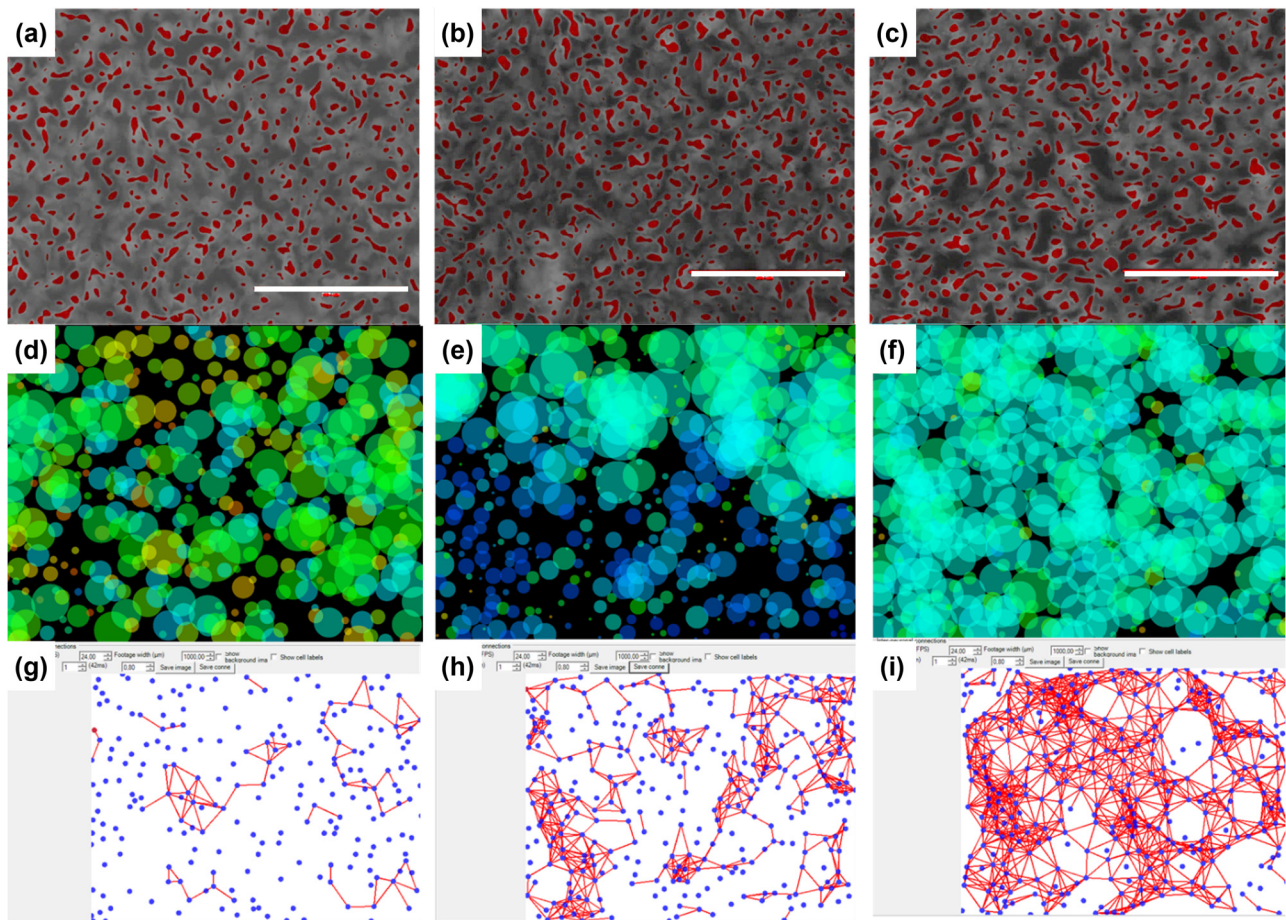


Fig. 4. Analysis example of calcium imaging recordings. Recordings are shown for differentiated SH-SY5Y neuroblastoma cells cultured on glass [(a), (d), and (g)], flat PDMS [(b), (e), and (h)], and nanogrooved PDMS [(c), (f), and (i)]. (a)–(c) Cell body detection (red, dark gray) superimposed on calcium imaging image. Scale bars denote 200  $\mu\text{m}$ . (d)–(f) Spatiotemporal map of spiking events for detected cells from (a)–(c). Circle size indicates the number of events, and the color indicates timepoints at which spiking events occurred. (g)–(i) Synchronous, correlated spiking events (red lines) between cells (blue dots) that are no greater than 50  $\mu\text{m}$  distance apart with a correlation of at least 0.8. These correlated spikes imply a connection between cells.

[Figs. 4(b), 4(e), and 4(h)], and nanogrooved PDMS [Figs. 4(c), 4(f), and 4(i)]. While the number of detected cells was comparable between the different substrates, the number of spiking events and the cell network connectivity increased for cells on nanogrooved PDMS.

An overview of the data derived from the quantitative analysis for both SH-SY5Y and hiPSCN calcium imaging experiments can be found in Table I in the supplementary material<sup>30</sup> and are visualized in Figs. 5 and 6, respectively. The results show that, of the SH-SY5Y cells, more than 80% of cells were active at 14 DIV and more than 70% of cells were active after 21 DIV, independent of the substrate. A trend is observed, in which relatively more SH-SY5Y cells show multiple spiking events for the PDMS substrates as compared to the glass substrate. Comparisons were made between groups for the number of events on either 14 DIV or 21 DIV. A Student's t-test was performed for each comparison between groups with a minimum of  $n=3$  samples, assuming normal distribution and independent samples and statistically significant differences at  $p \leq 0.05$ . No statistically significant differences were found as the tests resulted in  $p$  values  $>0.30$

for each possible comparison, except for the glass substrate as compared to the nanogrooved PDMS at  $\geq 3$  events and 21 DIV, which resulted in  $p = 0.19$ .

For the hiPSCN cultures, more than 25% of cells were active at 9 DIV and more than 40% of cells were active after 13 DIV. A trend is visible where the percentage of cells showing any activity was higher for cells on the nanogrooved PDMS. However, no statistically significant differences were found for the hiPSCN cultures with the same statistical test as performed for the cell activity as seen in the SH-SY5Y cell culture experiments, with tests resulting in  $p$  values  $>0.068$  for each possible comparison.

### 3. Neuronal cell network connectivity

The quantitative analysis, as discussed in Subsection III B 2, also derived quantitative data on the neuronal cell network connectivity [Figs. 4(g)–4(i)] for both SH-SY5Y and hiPSCN calcium imaging experiments. The values can be found in Table II in the supplementary material<sup>30</sup> and are visualized in Figs. 7 and 8 for SH-SY5Y cells and hiPSCNs, respectively.

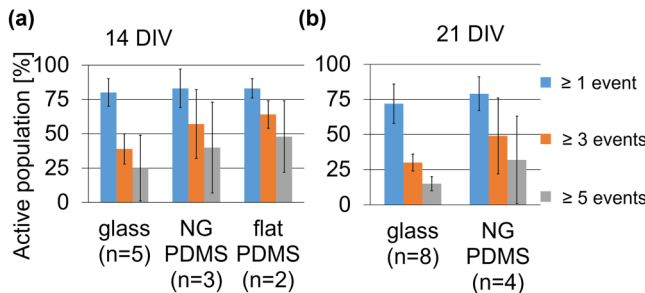


FIG. 5. Activity for differentiated SH-SY5Y cells on different substrates as derived from calcium imaging analysis. (a) Percentage of cell population showing  $\geq 1$  event (blue, left bar),  $\geq 3$  events (orange, middle bar), and  $\geq 5$  events (gray, right bar) at 14 DIV for flat glass, nanogrooved (NG) PDMS, and flat PDMS cell culture substrates. (b) Percentage of cell population showing  $\geq 1$  event (blue, left bar),  $\geq 3$  events (orange, middle bar), and  $\geq 5$  events (gray, right bar) at 21 DIV for flat glass and NG PDMS cell culture substrates. Error bars show standard deviation. The vertical axis title at (a) and the legend to the right of graph (b) apply to both graphs (a) and (b).

The results show that at 14 DIV, neuronal cell network connectivity for SH-SY5Y on flat PDMS substrates was  $\sim 2$  times higher compared to glass substrates and  $\sim 20$  times higher for nanogrooved PDMS substrates, compared to glass substrates. At 21 DIV, the connectivity decreased as compared to 14 DIV. While this trend is observed, the number of viable samples for this analysis was insufficient to calculate statistically significant differences.

The neuronal cell network connectivity for hiPSCNs was relatively limited at 9 DIV and for cells on glass substrates at 13 DIV, showing less than 100 connections, independent of the maximum distance between cells, as compared to 170 or more connections between cells on nanogrooved PDMS substrates. Using the same statistical test as used for the comparison in neuronal cell activity, we observe a statistically significant difference in the connectivity when comparing between glass substrates and nanogrooved PDMS at 13 DIV, with  $p = 0.033$  at  $50\mu\text{m}$  distance and  $p = 0.021$  at  $100\mu\text{m}$  distance.

Despite the limited data available, there is clearly a trend for cells on PDMS, preferably nanogrooved, to be more connected.

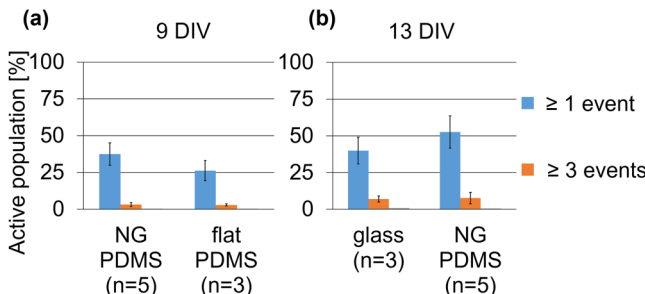


FIG. 6. Activity for hiPSCNs on different substrates as derived from calcium imaging analysis. (a) Percentage of cell population showing  $\geq 1$  event (blue, left bar) and  $\geq 3$  events (orange, right bar) at 9 DIV for NG PDMS and flat PDMS cell culture substrates. (b) Percentage of cell population showing  $\geq 1$  event (blue, left bar) and  $\geq 3$  events (orange, right bar) at 13 DIV for flat glass and NG PDMS cell culture substrates. Error bars show standard deviation. The vertical axis title at (a) and the legend to the right of graph (b) apply to both graphs (a) and (b).

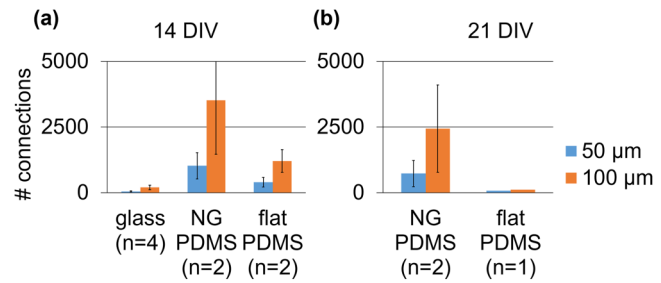


FIG. 7. As an indicator of the neuronal cell network connectivity for SH-SY5Y cells, the number of connections was calculated for simultaneous spiking events with a correlation of at least 0.8 and at maximum determined distances between the cells from calcium imaging recordings. The number of connections between SH-SY5Y cells is shown for (a) 14 DIV and (b) 21 DIV. The blue (left) bars denote connections at  $\leq 50\mu\text{m}$  and the orange (right) bars at  $\leq 100\mu\text{m}$ . Error bars show standard deviation. The vertical axis title at (a) and the legend to the right of graph (b) apply to both graphs (a) and (b).

To assess whether this increased connectivity would be directly visible as an increase in physical connections between cells relative to the number of cells, synaptophysin staining was performed on hiPSCNs as shown in Fig. 9. Calculation of the ratio between pixels showing the presence of synaptophysin against pixels showing cell nuclei resulted in a ratio of  $1.57 \pm 0.46$ ,  $1.68 \pm 0.39$ , and  $1.88 \pm 0.30$  for glass, nanogrooved PDMS, and flat PDMS substrates, respectively.

As there is no significant difference between the ratios of synapses to cell nuclei for the different substrates, the underlying reason for the increased connectivity of neuronal cells on PDMS substrates could be that the cells are more active, sending more signals across the same synapses instead of creating additional synapses. This can, however, only partially be explained due to cell activity, as only a trend but no significant increase in activity was seen in the neuronal cells depending on the substrate. Despite the successful retrieval of data from our experiments, the rate at which calcium

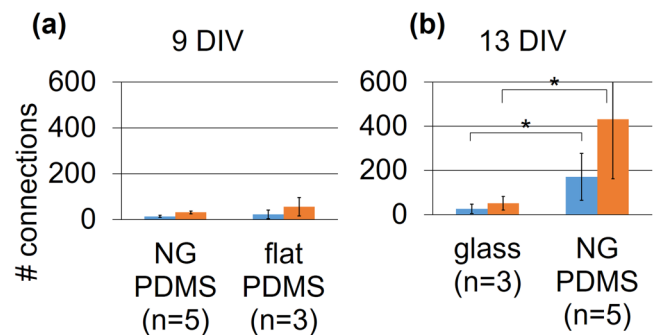


FIG. 8. As an indicator of the neuronal cell network connectivity for hiPSCNs, the number of connections was calculated for simultaneous spiking events with a correlation of at least 0.8 and at maximum determined distances between the cells from calcium imaging recordings. The number of connections between hiPSCNs is shown for (a) 9 DIV and (b) 13 DIV. The blue (left) bars denote connections at  $\leq 50\mu\text{m}$  and the orange (right) bars at  $\leq 100\mu\text{m}$ . Error bars show standard deviation. Statistical significant differences were calculated using the Student's t-test, assuming normal distribution and independent samples; \* indicates a statistically significant difference at  $p < 0.05$ . The vertical axis title at (a) and the legend to the right of graph (b) apply to both graphs (a) and (b).

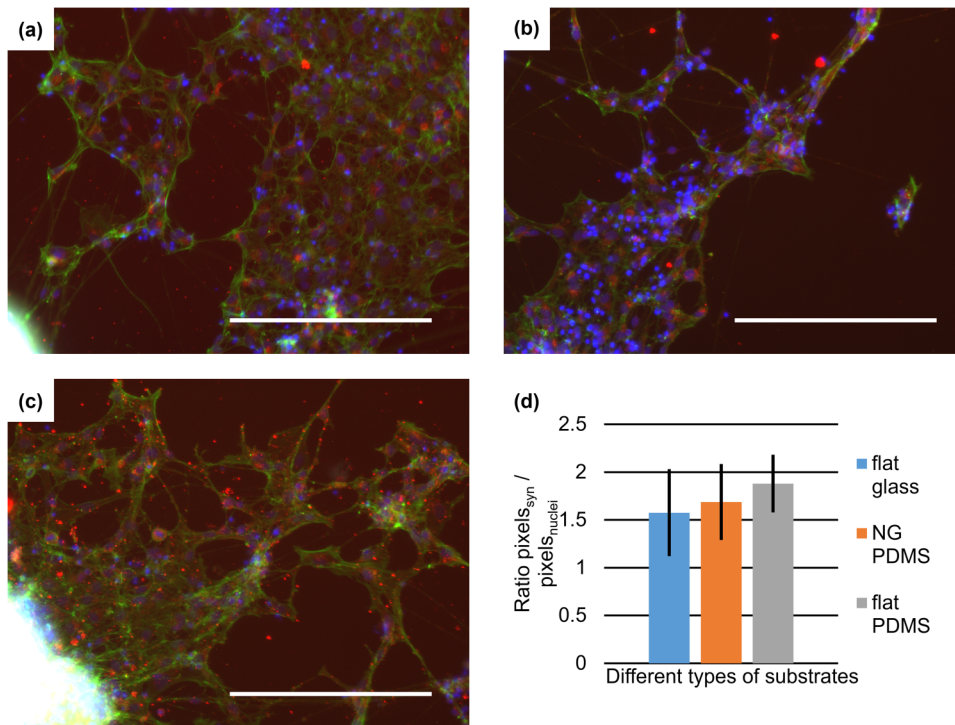


Fig. 9. Synaptophysin staining was performed to visualize synapses in hiPSCNs. Stainings were performed for hiPSCNs on (a) flat glass, (b) nanogrooved (NG) PDMS, and (c) flat PDMS. For (a)–(c), the synaptophysin staining is shown in red (medium gray dots), F-actin in green (light gray dots), and cell nuclei in blue (dark gray dots). All scale bars denote 200  $\mu$ m. (d) To assess whether the number of synapses would change depending on the substrate material or topography, the ratio between the synaptophysin staining and cell nuclei staining was calculated for  $n = 3$  images for each substrate type. This was conducted by counting pixels that showed synaptophysin in the red channel and cell nuclei in the blue channel of images and calculating the ratio. Error bars show standard deviation.

imaging is performed might pose limitations. Considering that the duration of intensity peaks in the calcium fluorophore Fluo-4 and the recordings from the microscope are in the seconds range while electrophysiological activity occurs within the microsecond range, alternatives such as cell transfection with fluorescent probes that act in the microsecond range and using real-time or high-speed frame rates may be used.<sup>24</sup>

Further, the success rate for loading calcium imaging dyes was low with regard to hiPSCN cultures, with samples often showing no calcium fluxes across cell membranes. In this study, we used standard culture media for SH-SY5Y and hiPSCNs to better maintain cell cultures during the calcium imaging process and to limit adverse effects from depleted nutrients and lower temperatures, as would happen when performed in different calcium imaging buffers such as Ringer's solution, PBS, or DPBS. Specifically, hiPSCN cultures quickly deteriorate when left under a microscope for recording, showing signs of cell death and cell detachment from the substrates within several minutes from the start of a recording. Therefore, alternative media or phosphate buffered saline solution should be explored to enhance cell activity, such as the introduction of high concentrations of calcium ions or potassium ions.

#### 4. Nanogroove influence on neuronal cell network form and function

From the data described in Sec. II B, trends that nanogrooved substrates increased electrophysiological activity

and connections within a neuronal cell network were observed for both cell types, albeit to a limited extent. Considering the effects of nanogrooved substrates on the guidance and formation of neuronal cells, especially the positive correlation between neuronal outgrowth guidance and neuronal differentiation, it is hypothesized that correlations can also be found between the nanotopographical guidance cues and neuronal network electrophysiological activity, thereby linking form and function of neuronal cell networks. These results, however, should be generated simultaneously in cell culture experiments for valid cross correlation and further investigation to be possible.

Further, we have seen for hiPSCNs that the guidance effect of the nanogrooves is relatively small at the DIV for which end-point measurements, such as calcium imaging, were performed [Fig. 3(d)]. In contrast, clear effects were seen in SH-SY5Y cell cultures [Figs. 3(a) and 3(b)]. The hiPSCNs tended to migrate on the substrate and form large clusters and many, long neuronal outgrowths within the first several days, whereas SH-SY5Y cells mostly remained as a monolayer on the substrates with shorter neuronal outgrowths. Extended observations for the first several days of cell culture might offer better insight into the benefits of nanotopography on hiPSCNs guidance and whether observations from SH-SY5Y and astrocytes from primary rat cortical cells, as mentioned in the Introduction, may also apply to hiPSCNs within this short time window.

### C. Nanotopographical, mechanical, and chemical cues in neuronal cell culture

As mentioned in the Introduction, cells react differently depending on the substrate, whether it is due to the dimensions of the underlying topography, the mechanical properties of the substrate, or the surface chemistry that allows for cell adhesion to a substrate. To better understand how these input parameters for the cellular environment impact the neuronal cells and their network, it is important to be able to study each independently to gain a clear understanding of the individual effects and their correlations. For instance, nanotopographical cues have been shown to synergize with chemical cues toward guiding neuronal outgrowths.<sup>25</sup> Understanding the mechanism and timing of these synergies is a key to enhance relevant environments, for both biological cell culture and engineering of cell model systems. Research in the brain-on-chip field also focuses on self-organization of neuronal cell cultures, especially with regard to the use of induced pluripotent stem cells and brainlike organoids.<sup>26–29</sup> However, changing environmental factors through reproducible micro- and nanofabrication technologies can aid in models that more accurately develop relevant tissue architecture.

Potentially, this allows us to tune the environment to better reflect differences between “healthy” and “diseased” tissue states by altering the topographical and mechanical properties, which we hypothesize can be achieved using the fabrication processes as shown in this study.

### IV. SUMMARY AND CONCLUSIONS

To summarize, this work demonstrates a method for a generalized replication protocol, in which nanogrooves on a nanoresist master are replicated into a primary COC mold, a secondary PDMS mold, and finally either into a PDMS or an Ostemem cell culture substrate. The replication has limited effects on the pattern replication, and results are similar to a sufficient degree for the nanogrooved PDMS and Ostemem substrates. Overall, our experiments further elucidate on the effect of nanotopographical and mechanical properties in advancing *in vitro* brain models both in form and function. Calcium imaging of SH-SY5Y cells and hiPSCNs has shown that nanogrooved PDMS substrates trend toward an increase in cellular electrophysiological activity and neuronal cell network connectivity, with significant effects at 13 DIV when comparing glass substrates with nanogrooved PDMS.

The results indicate, in conjunction with our previous findings on neuronal outgrowth guidance, that anisotropy as introduced by nanogrooved substrates can have a controllable and potentially beneficial influence on neuronal cell cultures.

### ACKNOWLEDGMENTS

This work was financially supported by the FET Proactive CONNECT project (Grant No. 824070) and the Eindhoven University of Technology. This work was also supported by ERC-STG project Grant No. 280281 and ERC-PoC project Grant No. 713732. The authors thank the members of the Microfab/lab at the Eindhoven University of Technology and the members of the MESA+ Institute at the University of Twente for their experimental support. In particular, the authors extend their thanks to Sijia Xie, who fabricated the nanoresist scaffolds and nanogrooved COC molds.

- <sup>1</sup>K. Duval, H. Grover, L.-H. Han, Y. Mou, A. F. Pegoraro, J. Fredberg, and Z. Chen, *Physiology* **32**, 266 (2017).
- <sup>2</sup>J. E. Sosa-Hernández *et al.*, *Micromachines* **9** (2018).
- <sup>3</sup>M. Akhmanova, E. Osidak, S. Domogatsky, S. Rodin, and A. Domogatskaya, *Stem Cells Int.* **2015**, 167025 (2015).
- <sup>4</sup>A. T. Nguyen, S. R. Sathe, and E. K. F. Yim, *J. Phys. Condens. Matter* **28**, 183001 (2016).
- <sup>5</sup>D. Hoffman-Kim, J. A. Mitchel, and R. V. Bellamkonda, *Annu. Rev. Biomed. Eng.* **12**, 203 (2010).
- <sup>6</sup>C. Simitzi, K. Karali, A. Ranella, and E. Stratakis, *ChemPhysChem* **19**, 1143 (2018).
- <sup>7</sup>G. Bugnicourt, J. Brocard, A. Nicolas, and C. Villard, *Langmuir* **30**, 4441 (2014).
- <sup>8</sup>Q. Huang, T. A. Elkhooly, X. Liu, R. Zhang, X. Yang, Z. Shen, and Q. Feng, *Colloids Surf. B Biointerfaces* **145**, 37 (2016).
- <sup>9</sup>I. Tonazzini, A. Cecchini, Y. Elgersma, and M. Cecchini, *Adv. Healthc. Mater.* **3**, 581 (2014).
- <sup>10</sup>Y. Kim, S. M. Meade, K. Chen, H. Feng, J. Rayyan, A. Hess-Dunning, and E. S. Ereifej, *Front. Neurosci.* **12**, 456 (2018).
- <sup>11</sup>S. Xie and R. Luttge, *Microelectron. Eng.* **124**, 30 (2014).
- <sup>12</sup>A. J. Bastiaens, S. Xie, and R. Luttge, *J. Vac. Sci. Technol. B* **36**, 06J801 (2018).
- <sup>13</sup>S. Xie, B. Schurink, F. Wolbers, R. Luttge, and G. Hassink, *J. Vac. Sci. Technol. B* **32**, 06FD03 (2014).
- <sup>14</sup>A. J. Bastiaens, S. Xie, D. A. M. Mustafa, J.-P. Frimat, J. M. J. den Toonder, and R. Luttge, *Front. Cell. Neurosci.* **12**, 1 (2018).
- <sup>15</sup>E. Moonen, R. Luttge, and J. P. Frimat, *Microelectron. Eng.* **197**, 1 (2018).
- <sup>16</sup>D. Sticker, M. Rothbauer, S. Lechner, M.-T. Hehenberger, and P. Ertl, *Lab Chip* **15**, 4542 (2015).
- <sup>17</sup>N. Sandström, R. Z. Shafagh, A. Vastesson, C. F. Carlborg, W. Van Der Wijngaart, and T. Haraldsson, *J. Micromech. Microeng.* **25** (2015).
- <sup>18</sup>D. Nečas and P. Klapetek, *Cent. Eur. J. Phys.* **10**, 181 (2012).
- <sup>19</sup>S. Dwane, E. Durack, and P. A. Kiely, *BMC Res. Notes* **6**, 366 (2013).
- <sup>20</sup>H. Teppola, J. R. Sarkkanen, T. O. Jalonen, and M. L. Linne, *Neurochem. Res.* **41**, 731 (2016).
- <sup>21</sup>M. Encinas, M. Iglesias, Y. Liu, H. Wang, A. Muhausen, V. Ceña, C. Gallego, and J. X. Comella, *J. Neurochem.* **75**, 991 (2000).
- <sup>22</sup>L. Agholme, T. Lindström, K. Kågedal, J. Marcusson, and M. Hallbeck, *J. Alzheimers Dis.* **20**, 1069 (2010).
- <sup>23</sup>J. Schindelin *et al.*, *Nat. Methods* **9**, 676 (2012).
- <sup>24</sup>C. Grienberger and A. Konnerth, *Neuron* **73**, 862 (2012).
- <sup>25</sup>C. Miller, S. Jeftinija, and S. Mallapragada, *Tissue Eng.* **8**, 367 (2002).
- <sup>26</sup>W. K. Raja, A. E. Mungenast, Y.-T. Lin, T. Ko, F. Abdurrob, J. Seo, and L.-H. Tsai, *PLoS One* **11**, e0161969 (2016).
- <sup>27</sup>M. A. Lancaster *et al.*, *Nature* **501**, 373 (2013).
- <sup>28</sup>R. K. Das and O. F. Zouani, *Biomaterials* **35**, 5278 (2014).
- <sup>29</sup>T. Kadoshima, H. Sakaguchi, T. Nakano, M. Soen, S. Ando, M. Eiraku, and Y. Sasai, *Proc. Natl. Acad. Sci.* **110**, 20284 (2013).
- <sup>30</sup>See supplementary material at <https://doi.org/10.1111/1.5119687> for data derived from calcium imaging analysis and hiPSCs culture on Ostemem.